ENVIRONMENTAL RESEARCH
LETTERS

LETTER • OPEN ACCESS

Arctic as the ‘radiator fins’ of Earth in a warming climate

To cite this article: Han Huang and Yi Huang 2024 *Environ. Res. Lett.* **19** 054032

View the article online for updates and enhancements.

IOP Publishing Environ. Res. Lett. 19 (2024) 054032 https://doi.org/10.1088/1748-9326/ad3e17

ENVIRONMENTAL RESEARCH
LETTERS

RECEIVED
24 December 2023

REVISED
24 March 2024

ACCEPTED FOR PUBLICATION
12 April 2024

PUBLISHED
23 April 2024

LETTER

Arctic as the 'radiator fins' of Earth in a warming climate

Han Huang* and Yi Huang*

Department of Atmospheric and Oceanic Sciences, McGill University, Montreal, Canada
* Authors to whom any correspondence should be addressed.

E-mail: han.huang2@mail.mcgill.ca and yi.huang@mcgill.ca

Keywords: radiator fin, earth's energy budget, climate change

Supplementary material for this article is available online

Abstract

Earth radiates thermal radiation to balance the solar radiation it receives. Central to understanding climate change is how the radiation energy budget adjusts both globally and locally to external and internal forcing. In the past 18 years, satellite observations reveal a distinct positive trend of the Earth thermal radiation in the Arctic, which acts to radiate excess heating accumulating in the climate system to the space during global warming, i.e. a radiator fin region in a warming climate. Compared with other regions such as the tropics, the prominent trend in the Arctic results from a stronger surface and atmospheric warming and a less offsetting greenhouse effect of water vapor. Spectral decompositions further show the increase of thermal emission in the Arctic mainly originates from the far-infrared and mid-infrared window region and affirms the unbalanced radiative responses to temperature and humidity changes in these two spectral regions account for the unique thermal radiation trend in the Arctic.

1. Introduction

The Earth climate can in many ways be considered a 'furnace-radiator-fin' system [1], with excessive heat being produced in the furnace regions and radiated away in the radiator-fin regions. In terms of the mean climate, the 'furnace' and 'radiator fin' have been used to describe the convective and subsidence regions, respectively, in the tropics, where the unstable atmospheric condition leading a runaway greenhouse in the 'furnace' region is stabilized by exporting heat to the 'radiator fin' region [1]. In the context of global warming, it has been of central interest in climate research to identify radiator fin regions and mechanisms facilitating the cycling and loss of energy to cool down the warming climate. For example, an Iris effect was hypothesized to modulate the outgoing longwave radiation (OLR) through changing water vapor and cloud amounts in analogy to an eye's iris [2], although no clear evidence has been found for such a negative climate feedback [3]. Questions remain: does the Earth in a warming climate have radiator fins, and if it does, where do they exist?

The OLR is key to identifying radiator fins (e.g [4]). The earth climate is shaped by the balance between the OLR and the absorbed solar radiation at the top of the atmosphere (TOA) [5–7]. Previous studies discovered an imbalance of the global mean radiation energy budget mainly caused by enhanced absorption of solar radiation [8–11]. This makes it increasingly important to elucidate how the OLR responds at both global and regional scales to counteract more absorbed solar radiation.

In this letter, we report that, based on the start-of-the-art earth satellite observations, the Arctic appears to be a prominent, if not the only, radiator-fin region to radiate increasing amount of OLR during global warming (figure 1), and, using radiative transfer modeling, we elucidate that this is due to an unparalleled effect of the surface and atmospheric warming and weak water vapor greenhouse effect, which leads to substantial OLR increase in the Arctic, distinguishing it from the rest of the globe.

2. Satellite-observed OLR trend

To identify the radiator-fin regions, we use the Balance and Filled dataset of the Clouds and Earth's Radiant Energy System Energy satellite (CERES EBAF) [12] to calculate the geographic distributions of OLR trends during January 2002–December 2019. The OLR trend at each location is calculated by a linear regression of deseasonalized OLR monthly anomaly time series. Figure 1(a) shows that satellite observed OLR trend over the globe and reveals that the Arctic region (70 N–90 N) shows a remarkable increase of OLR in this period, at a rate of 1.20 ± 0.84 W m^{-2} decade^{-1}. The zonal mean OLR trend pattern (figure 1(b)) further affirms that the Arctic is exceptional in that this is the only region where the trend magnitude clearly exceeds the uncertainty, identifying the Arctic to be a radiator-fin region in a warming climate. In comparison, the global mean OLR trend is found to be 0.17 ± 0.18 W m^{-2} decade^{-1}, resulting from the non-robust trends in other regions such as the tropics (table 1). The insignificant global mean trend found here is in consistency with several previous studies [8, 13, 14]. Such comparison bears an interesting and important question—why does the Arctic region exhibit a strong OLR increase while the other regions do not?

3. Geophysical variable trends

To answer the question above, we first investigate the factors that control the OLR from radiative transfer point of view. We use the reanalysis data from the fifth generation of European Center for Medium-Range Weather Forecasts atmospheric reanalysis (ERA5) [15] to examine the trends in surface temperature, air temperature, atmospheric water vapor (figure 1) and cloud cover (figure S1) in three regions: the global, tropics (30 N–30 S), and Arctic (70 N–90 N). The global and tropical means are used to make comparison with the Arctic and to better illustrate the cause of unique OLR trend in the Arctic, with one representing the averaged change over the globe (global mean) and another representing the region with much different atmospheric state (the tropics).

In contrast to the OLR which shows a significant trend only in the Arctic, we find significant trends in the state variables not only in the Arctic but also in the tropics and for the global mean (figures 1(c)–(f) and S1). The surface temperature change exhibits a well-known amplified warming in the Arctic [16–18], although statistically significant warming also emerges in the middle latitudes and the south pole (figure 1(d)), which suggests that the surface warming alone cannot explain the distinct OLR increase in the Arctic. The air temperature and specific humidity increases in the Arctic manifest a bottom-heavy feature, while their increases in the other two regions show a vertically more uniform pattern (figure 1(e)). Compared with the global or tropical mean, the lower troposphere in the Arctic experiences a much stronger warming (figure 1(e)). In terms of water vapor concentration change, although the fractional changes in the Arctic are 3–4 times stronger than that in the tropics and global mean, especially in the lower troposphere, it is worth noting that the absolute water vapor concentration in the Arctic atmosphere is about one to two orders of magnitude smaller than that in the tropics and the global mean, meaning that the Arctic is still much drier than the tropics in the warming climate. For the clouds, the total cloud cover changes mostly occur in the tropics, with increasing cloudiness in the Eastern Pacific and reduction in the Western Pacific (figure S1(a)), which correspond well to the regional OLR changes in these regions (figure 1(a)) but their compensation neutralizes the change in the tropical mean OLR (table 1). The findings here are consistent with [19], which investigated the clear-sky OLR trend in the Arctic.

In short, significant changes in surface and atmospheric state variables are found in the Arctic, as well as other regions globally. This suggests that the distinct OLR increase in the Arctic region cannot be attributed to the changes in any variable (such as surface temperature or air temperature) alone. Therefore, the respective contributions of multiple factors to the OLR change warrant further investigations.

4. Quantifying the causes of OLR increase

To measure the respective contributions of different surface and atmospheric variables to the OLR change and identify the reason for a unique OLR increase in the Arctic region, we use the Rapid Radiative Transfer Model (GCM version, RRTMG) [21] to simulate the OLR changes of the same period as the CERES observation.

Conceptually, the OLR change can be decomposed to the contributions of the radiative forcing of Greenhouse-Gases (GHGs) and other radiative responses [22–25]:

$$\Delta R = \underbrace{\Delta R_{\mathrm{GHG}}}_{\text{Radiative forcing}} + \underbrace{\Delta R_{ts} + \Delta R_{ta} + \Delta R_q + \Delta R_c}_{\text{Radiative responses}}. \tag{1}$$

In this decomposition, the radiative forcing term ΔR_{GHG} includes the contributions of well-mixed GHGs such as CO_2, CH_4, N_2O (ΔR_{WMG}), and the nonuniform GHG: O_3 (ΔR_{O3}). The radiative response term is contributed by the changes in surface temperature (ΔR_{ts}), air temperature (ΔR_{ta}), atmospheric water vapor (ΔR_q) and clouds (ΔR_c). Radiative forcing ΔR_{GHG} is calculated by the difference of two RRTMG simulations with and without GHGs changes, and radiative responses are calculated using the kernel method [26–28] (see data and methods section). The RRTMG simulations are validated against the CERES (figure S2). It is worth noting that the overall OLR change, radiative forcing and radiative responses in equation (1) are respectively regressed on their timeseries to obtain the corresponding trends. For simplicity, we use the terms in equation (1) to directly represent their trends in the following and denote them as radiative forcing contribution and radiative response contribution.

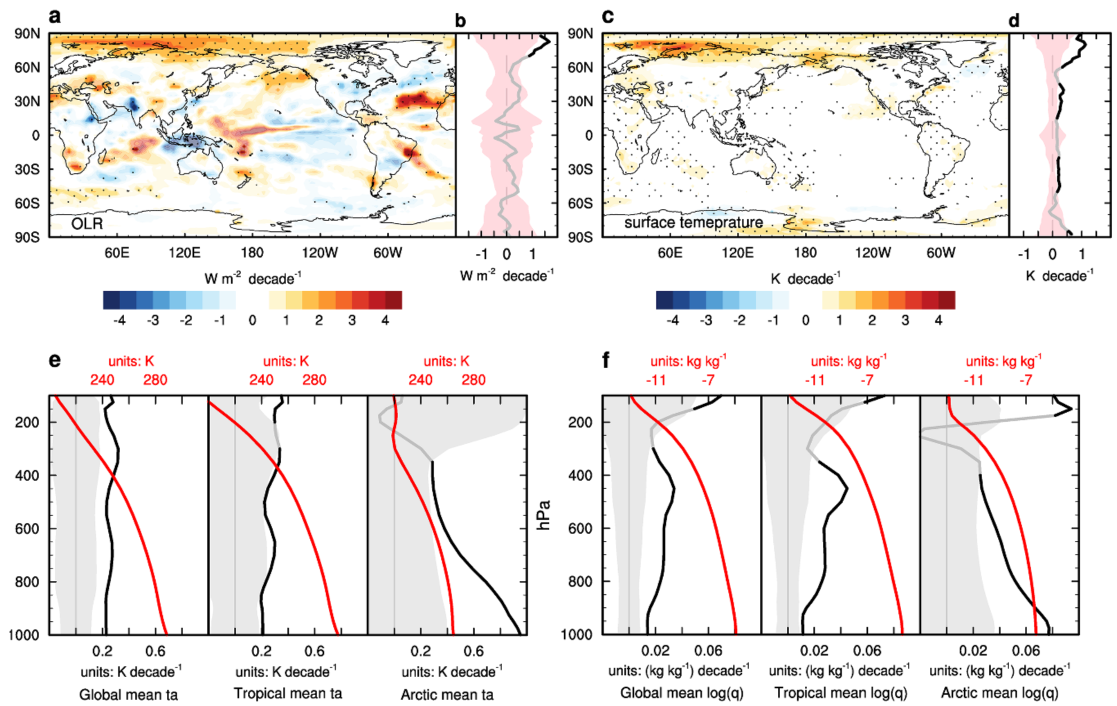

Figure 1. Climate trends in OLR and other surface and atmospheric variables. (a) Geographic distribution and (b) zonal mean pattern of OLR trend from CERES; (c) and (d) the same as (a) and (b) but for surface temperature from ERA5, (e) regional mean vertical distribution of air temperature (*ta*) trend (black line) and its climatological value (red line); (f) the same as (e), but for atmospheric water vapor (*q*). The dotted areas in panels (a) and (c) indicate the regions with trends significant at the 95% confidence level; the pink shadings in panels (b) and (d), and grey shadings in panels (e) and (f) indicate the uncertainty interval of the trends at the same confidence level (see data and methods section). Black (grey) lines in (b), (d), (e) and (f) represent significant (insignificant) trends. OLR = outgoing longwave radiation, CERES = Cloud and Earth's Radiant Energy System. ERA5 = the fifth generation of European Center for Medium-Range Weather Forecasts atmospheric reanalysis. OLR is defined as upward positive and positive trend means OLR increase. Atmospheric water vapor is presented as the logarithm of specific humidity, log (q).

Table 1. OLR trends in the global mean, tropical mean and Arctic mean from CERES observations and RRTMG simulations.

	W m^{-2} decade^{-1}	Arctic mean	Tropical mean	Global mean
Observation	$\Delta R_{\mathrm{CERES}}$	1.20 ± 0.84	0.04 ± 0.34	0.17 ± 0.18
RRTMG-simulation	$\Delta R_{\mathrm{RRTMG}}$	1.28 ± 0.82	-0.31 ± 0.29	0.03 ± 0.14
	ΔR_{GHG}	-0.19 ± 0.09	-0.35 ± 0.12	-0.30 ± 0.09
	ΔR_{c}	0.02 ± 0.25	-0.32 ± 0.18	-0.13 ± 0.13
	nonΔR_c	1.44 ± 0.76	0.27 ± 0.27	0.39 ± 0.21
	ΔR_{ts}	0.63 ± 0.28	0.15 ± 0.12	0.18 ± 0.08
	$\Delta R_{ta} + \Delta R_q$	0.82 ± 0.59	0.12 ± 0.18	0.22 ± 0.14

$\Delta R_{\mathrm{CERES}}$ = OLR trend from CERES observations, $\Delta R_{\mathrm{RRTMG}}$ = OLR trend from RRTMG simulations, ΔR_{GHG} = OLR trend due to Greenhouse-Gas change, nonΔR_c = OLR trend due to non-cloud component changes, ΔR_c = OLR trend due to cloud change, ΔR_{ts} = OLR trend due to surface temperature change, $\Delta R_{ta} + \Delta R_q$ = OLR trend due to both atmospheric temperature and water vapor changes. CERES = Cloud and Earth's Radiant Energy System, RRTMG = Rapid Radiative Transfer Model—GCM version, global mean = averaged over the whole globe with area weights, tropical mean = averaged from 30 N to 30 S, Arctic mean = from 70 N to 90 N. Uncertainties are calculated by the Weatherhead method [20] (see data and methods section). Positive (negative) trend means OLR increase (decrease).

For radiative forcing contribution, the global mean value is around −0.30 W m^{-2} decade^{-1} (figure 2(a)), consistent with previous estimations [14]. The contribution in the tropics and Arctic is relatively stronger and weaker compared with the global mean value, due to the atmospheric state dependency of the forcing [29, 30]. Compared to the overall OLR change, the radiative forcing contribution is much less and of the opposite sign in the Arctic. While in the tropics or for global

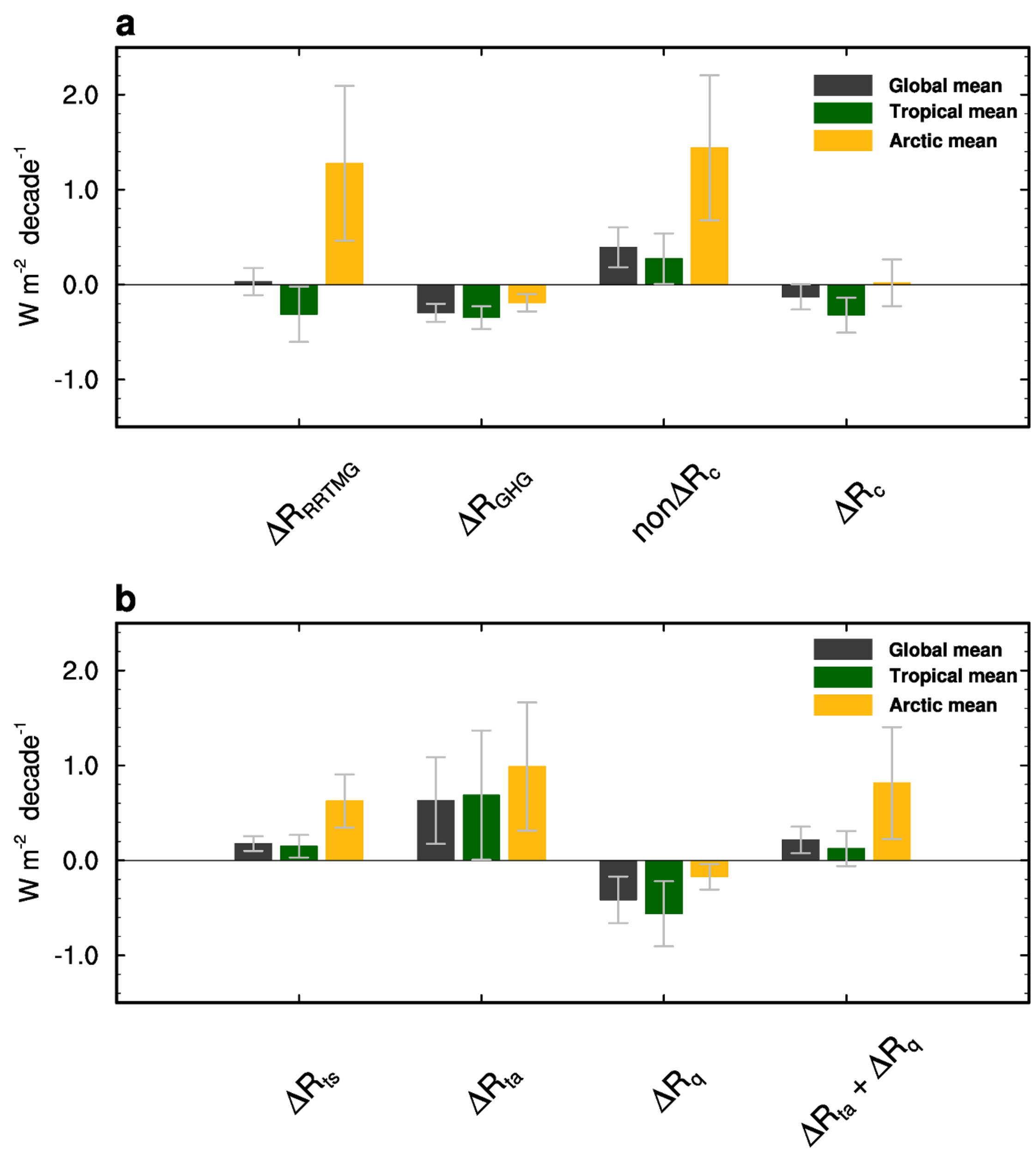

Figure 2. Decomposition of the OLR trend. (a) Component contributions to OLR trend calculated by RRTMG and kernel method; (b) further decomposed non-cloud contributions. Global mean is the area-weighted average value across the globe. Tropical mean is averaged from 30 N to 30 S. Arctic mean is from 70 N to 90 N. Grey vertical bars are the uncertainties calculated by the Weatherhead method [20] (see data and methods section). $\Delta R_{\mathrm{RRTMG}}$ = OLR trend from RRTMG simulations, ΔR_{GHG} = OLR trend due to Greenhouse-Gas change, nonΔR_c = OLR trend due to non-cloud component changes, ΔR_c = OLR trend due to cloud change = OLR trend due to surface temperature change, ΔR_{ta} = OLR trend due to atmospheric temperature change, ΔR_q = OLR trend due to water vapor change, $\Delta R_{ta} + \Delta R_q$ = OLR trend due to both atmospheric temperature and water vapor changes, OLR = outgoing longwave radiation, RRTMG = rapid radiative transfer model—GCM version. Upward positive is defined for all terms.

mean, the fractional contribution of radiative forcing is much stronger due to small total OLR change.

The non-cloud radiative responses in the Arctic make substantial contributions to the OLR increase, which is consistent with previous findings [19]. Among all non-cloud variables, the surface temperature and air temperature increase contribute most to the OLR increase, with the contribution of air temperature slightly higher than that of surface temperature (figure 2(b)). The greenhouse effect of the moistening in the atmosphere is much weaker compared with the temperature contribution (figure 2(b)). As noticed earlier in figure 1(b), this is due to the low water vapor concentration in the Arctic even in a warmer climate, despite the much stronger local moistening trend. The findings here are consistent with [19], that the temperature effect makes a major contribution to the OLR trend in the Arctic. But different from their finding that the surface temperat-

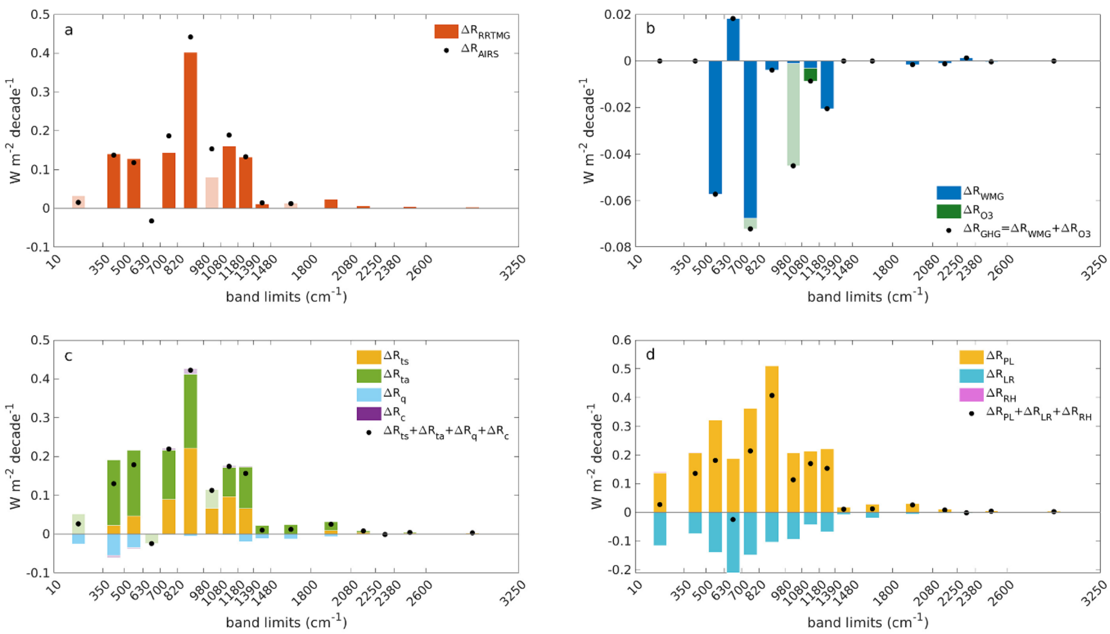

Figure 3. Spectrally-decomposed OLR trends in the Arctic. (a) total spectral trend, (b) GHG forcing contributions, (c) atmospheric and surface response contributions, (d) similar to (c) but recombined to quantify Planck, lapse rate and relative humidity effects. The lightened color bars in each panel represent statistically insignificant trends and the normal color bars, significant trends. $\Delta R_{\mathrm{RRTMG}}$ = OLR trend from RRTMG simulations, ΔR_{AIRS} = OLR trend from AIRS observation, ΔR_{GHG} = OLR trend due to GHG change, ΔR_{WMG} = OLR trend due to well-mixed GHGs change, ΔR_{O3} = OLR trend due to ozone change, ΔR_c = OLR trend due to cloud change, ΔR_{ts} = OLR trend due to surface temperature change, ΔR_{ta} = OLR trend due to air temperature change, ΔR_q = OLR trend due to atmospheric water vapor change, ΔR_{PL} = OLR trend due to Planck effect, ΔR_{LR} = OLR trend due to lapse rate change, ΔR_{RH} = OLR trend due to relative humidity change. OLR = outgoing longwave radiation, AIRS = Atmospheric Infrared Sounder, RRTMG = rapid Radiative Transfer Model GCM version, GHG = Greenhouse-Gas, AIRS = Atmospheric Infrared Sounder. Upward positive is defined for all terms.

ure contributes the most in clear sky, we find that it is the air temperature that makes the strongest contribution in all sky, due to clouds masking the surface contribution.

In comparison, the contributions of surface temperature and water vapor in the tropics and for global mean are much different from those in the Arctic. Taking the tropics as an example, high climatological water vapor concentration (figure 1(f)) and relatively weaker surface warming trend (figure 1(b)) lead to a weak positive contribution of surface temperature. Meanwhile, the increase of tropical water vapor concentration strongly dampens the OLR increase and offsets the temperature effect, leading to a small OLR trend (figure 2(b)). The sum of air temperature and water vapor contributions in figure 2(b) shows a shear contrast between the tropics and Arctic.

Clouds make no prominent contribution to OLR change in the Arctic and a weak negative contribution for the tropics and global mean. In the Arctic, this results from compensating effects of a cover increase in the near-surface layer and decrease in the mid-to-high troposphere (figure S1(c)), while in the tropics this results from geographically compensating cloud changes noted earlier.

In summary, the decomposed contributions of radiative forcing and responses to OLR change evidence that the robust OLR increase in the Arctic region is due to an unparalleled temperature warming effect and a weak dampening effect of water vapor compared with other regions, i.e. the distinct, unbalanced radiative responses to the temperature and humidity change.

5. Spectral contributions to OLR change

Spectral decompositions provide further insights on how the OLR changes. Figure 3 shows the spectral OLR trend in the Arctic. The Arctic total spectral trend is validated against the Atmospheric Infrared Sounder (AIRS) Level 3 spectral observation [31] (figure 3(a)) and is mainly from the contributions in the far-infrared (FIR) band (10–500 cm^{-1}) and the window region (700–1080 cm^{-1}).

The GHG increase reduces the OLR mainly at the wings of the 667 cm^{-1} (15 μm) CO_2 absorption band (figure 3(b)). While in the CO_2 absorption center, the OLR shows an increasing trend. This is because the OLR in the CO_2 absorption center mainly originates from the stratosphere and with CO_2

increase, the emitting layer is elevated to a higher and warmer altitude [32] and thus leads to an OLR increase. The spectral OLR signatures of the GHG forcing quantified here corroborate the CO_2 effects postulated in earlier studies [33, 34]. In addition, another noteworthy finding for the OLR change is the O_3 increase during this period, without which one cannot explain the decrease of OLR in its absorption band at 1040 cm^{-1} (9.6 μm).

The spectral results also vividly illustrate the contrasting behaviors in the Arctic and Tropics in terms of the compensation between the temperature and water vapor effects noted earlier (figures 3 and S3). In the Arctic, not only does the surface and air temperature warming lead to a greater increase of OLR in the H_2O absorption band in the far-infrared (FIR, $<$500 cm^{-1}), but the temperature effect is much less offset by increased trapping (reduction) of OLR caused by the atmospheric moistening (figure 3(c)). The spectral signals disclosed here indicate the usefulness of FIR measurements for detecting and attributing climate change, which can be observationally validated by the planned FIR satellite missions [35–37] to fly in near future. The spectral trends detected in this section agree well with the findings of [19], where the spectral trend of clear-sky OLR was analyzed in different seasons.

If organizing the water vapor and temperature-induced spectral OLR changes to Planck, lapse rate (LR) and relative humidity change (RH) effects (figure 3(d)), according to the decomposition Method [38] (see Data and Method section) and using the aid of spectral kernels [39], it is clear that the prominent increase of OLR in Arctic compared to tropics is largely contributed by the Planck term, which further affirms that the unique increase of OLR in the Arctic region is due to the distinct radiative sensitivity of OLR to temperature and water vapor changes in this region and not caused by different vertical patterns or non-thermodynamically-constrained (varying RH) changes of them.

6. Discussion

Satellite observations analyzed here reveal the Arctic to be a unique 'radiator fin' region in the warming climate, which shows a robust increasing trend of OLR in the past eighteen years and acts to radiate away the excessive heat in the climate system accumulated by an increase of the net solar radiation absorbed by Earth.

Our modeling analyses suggest that the unparalleled increase of OLR in the Arctic is mainly caused by a strong surface and atmosphere warming and a low background water vapor concentration in the past 18 years. The temperature warming effect leads to a substantial increase in OLR in the Arctic and the low background water vapor concentration allows transmission of increased thermal radiation to space, both of which contribute to a distinct OLR increase in the Arctic. In comparison, the abundant water vapor and stronger greenhouse effect in the tropics neutralize the OLR increase caused by temperature warming.

The spectral decomposition of the OLR trend discloses that the increase of Arctic OLR mainly occurs in the mid-infrared atmospheric window and far-infrared region, both of which are observationally verifiable. This warrants the observation of OLR and its spectrum, to monitor whether the continued warming and moistening in the Arctic will reduce the effectiveness of the 'radiator fin', which may have important implications for both the local and global radiation energy budget.

Data availability statement

The ERA5 datasets can be accessed through the ECMWF website: ERA5 hourly data on single levels from 1940 to present (copernicus.eu). The CERES datasets are available at: CERES Data Products—CERES (nasa.gov). The ERA5-based radiative kernels can be downloaded at Huang and Huang [40].

The data that support the findings of this study [41] are openly available at the following URL/DOI: https://doi.org/10.17632/wxdd574x8c.

Acknowledgments

We acknowledge the grants from the Natural Sciences and Engineering Research Council of Canada (RGPIN-2019-04511) and the Fonds de Recherché Nature et Technologies of Quebec (2021-PR-283823) that supported this research.

Author contributions

Y H conceived the idea of Arctic radiator fins. H H and Y H co-designed the numerical experiments and satellite data analyses. H H conducted the simulations and analyses. H H and Y H co-wrote the manuscript.

Conflict of interest

The authors declare that they have no conflict of interests.

Appendix

Data and Methods

Observations: we use two satellite observations in this work. One is the Cloud and Earth's Radiant Energy System Energy Balance and Filled Edition 4.2 [12] (CERES EBAF Ed4.2) from January 2002 to December 2019. Another is from Atmospheric Infrared Sounder (AIRS) Level 3 spectral OLR [31] from January 2003 to December 2019. Both datasets are interpolated to the horizontal grids with resolution of 2.5 deg × 2.5 deg (the same as ERA5 reanalysis data used in RRTMG simulations). CERES only provides broadband OLR values and AIRS data contains the spectral OLR value with the band interval of 10 cm^{-1} from wavenumber 15 cm^{-1}–1995 cm^{-1}.

Monthly mean OLR values are used and the anomalies are calculated as the deviations from the climatological monthly value (i.e. deseasonalized timeseries) to calculate the OLR trend.

Trend and Uncertainty: Consider a linear regression model,

$$\hat{y} = a * t + b \tag{M1}$$

where $\hat{y}$ is the estimated anomalous timeseries of the variable of interest (e.g. OLR anomaly, or its radiative forcing or response component). t is the time span of the timeseries. a and b are the linear regression coefficient and y-intercept, respectively. As the autocorrelation of a timeseries can affect the detection of linear trends, we adopt the method proposed by [20] to calculate the standard deviation of linear regression coefficient a as,

$$\sigma = \sqrt{\frac{\sum_{i=1}^{n} (y_i - \widehat{y_i})^2}{(n-2)\sum_{i=1}^{n} (t_i - \bar{t})^2} \frac{1+\Phi}{1-\Phi}} \tag{M2}$$

where y_i and $\widehat{y_i}$ are the truth and estimated value at the ith time instance. n is the total time instances (the length of y timeseries). t_i is the ith time instance and $\bar{t}$ is the mean value of t. Φ is the auto-correlation coefficient of y. Hence, using a 95% confidence level, we consider the trend to be significant if the trend magnitude of a is over 2σ; otherwise insignificant.

Models: we use the rapid-radiative-transfer-model GCM version (RRTMG) and 4-times daily instantaneous ERA5 profiles to simulate the OLR for the same period as CERES observations. The required inputs such as surface temperature, air temperature, water vapor, ozone concentration, cloud cover and cloud water path are from ERA5, and the required effective radii of cloud droplets are from the 3-hourly synoptic TOA and surface fluxes and cloud product of CERES [42]. A random cloud overlapping scheme is adopted for all-sky simulations.

The RRTMG can not only output broadband OLR but also 16 spectral band-integrated values, spanning from 10 cm^{-1} to 3250 cm^{-1}. To validate the RRTMG spectral results, we convert the AIRS data to the same band limits as RRTMG (figures 3 and S3).

Radiative forcing: The total OLR trend can be decomposed into contributions of radiative forcing and radiative responses (equation (1)). To quantify the radiative forcing induced by GHGs emissions, we run RRTMG simulations of OLR with and without changes in GHGs and use the difference between these two simulations to calculate the radiative forcing. The GHG concentrations are taken from the National Oceanic and Atmospheric Administration Global Monitoring Laboratory [43, 44].

Radiative responses and kernel method: The non-cloud radiative responses in equation (1) are diagnosed by the kernel method,

$$\Delta R_x = K_x * \Delta x \tag{M3}$$

ΔR_x is the response variable x change induced OLR change. K_x is the broadband radiative kernel of variable x, which represents the radiative sensitivity of OLR to x perturbation. Δx is the deseasonalized anomaly of x. The cloud response is calculated using the adjusted cloud radiative effect method [27],

$$\begin{aligned}\Delta R_c = (\Delta R - \Delta R^o) - (\Sigma \Delta R_x - \Sigma \Delta R_x^o) \\ - (\Delta R_{\mathrm{GHG}} - \Delta R_{\mathrm{GHG}}^o)\end{aligned} \tag{M4}$$

where the superscript o represents quantities in clear sky. ΔR and ΔR^o are the deseasonalized OLR timeseries simulation by RRTMG in all sky and clear sky, respectively. $\Sigma \Delta R_x$ and $\Sigma \Delta R_x^o$ are the sum of non-cloud radiative responses in all sky and clear sky, respectively. ΔR_{GHG} and $\Delta R_{\mathrm{GHG}}^o$ are the radiative forcings in all sky and clear sky, receptively. In this work, the broadband ERA5 kernels developed by [28] are used for the calculation.

The spectral radiative response can be calculated using similar method but with spectral radiative kernel. Here we use a set of spectral radiative kernel based on ERA5 reanalysis [39], which is also generated by RRTMG and has the same band configurations as the simulations used in this study. The spectral non-cloud radiative responses are calculated as,

$$\Delta R_x^i = K_x^i * \Delta x \tag{M5}$$

where K_x^i is the spectral radiative kernel of variable x in the ith band and ΔR_x^i is the corresponding responses of x in the ith band. The broadband response ΔR_x is the sum of spectral responses in all 16 bands ($\sum_{i=1}^{16} \Delta R_x^i$).

Based on Held and Shell [38], the radiative responses induced by the temperature and water vapor changes can be organized using the relative humidity as a state variable,

$$\Delta R_{PL} = \left(K_{ts} + K_{ta} + K_q\right) * dts \tag{M6}$$

$$\Delta R_{\mathrm{LR}} = \left(K_{ta} + K_q\right) * (dta - dts) \tag{M7}$$

$$\Delta R_{\mathrm{RH}} = K_q * (dq - dta) \tag{M8}$$

in which ΔR_{PL} is the Planck contribution, i.e. the contribution to OLR change by a vertically uniform temperature change. ΔR_{LR} is the lapse rate contribution, i.e. the contribution to OLR change due to the vertically non-uniform temperature change. ΔR_{RH} is the contribution to OLR due to relative humidity change. Following equation (M5), these contributions can also be decomposed into spectral bands (figure 3(d)).

ORCID iDs

Han Huang https://orcid.org/0000-0002-9143-6453
Yi Huang https://orcid.org/0000-0002-5065-4198

References

[1] Pierrehumbert R T 1995 Thermostats, radiator fins, and the local runaway greenhouse *J. Atmos. Sci.* **52** 1784–806
[2] Lindzen R S, Chou M-D and Hou A Y 2001 Does the earth have an adaptive infrared iris? *Bull. Am. Meteorol. Soc.* **82** 417–32
[3] Sherwood S C *et al* 2020 An assessment of Earth's climate sensitivity using multiple lines of evidence *Rev. Geophys.* **58** e2019RG000678
[4] McKim B A, Jeevanjee N and Vallis G K 2021 Joint dependence of longwave feedback on surface temperature and relative humidity *Geophys. Res. Lett.* **48** e2021GL094074
[5] Kiehl J T and Trenberth K E 1997 Earth's annual global mean energy budget *Bull. Am. Meteorol. Soc.* **78** 197–208
[6] Trenberth K E, Fasullo J T and Kiehl J 2009 Earth's global energy budget *Bull. Am. Meteorol. Soc.* **90** 311–24
[7] Stevens B and Schwartz S E 2012 Observing and modeling Earth's energy flows *Surv. Geophys.* **33** 779–816
[8] Raghuraman S P, Paynter D and Ramaswamy V 2021 Anthropogenic forcing and response yield observed positive trend in Earth's energy imbalance *Nat. Commun.* **12** 4577
[9] Trenberth K E and Fasullo J T 2009 Global warming due to increasing absorbed solar radiation *Geophys. Res. Lett.* **36** 7
[10] Stephens G L, Hakuba M Z, Kato S, Gettelman A, Dufresne J-L, Andrews T, Cole J N, Willen U and Mauritsen T 2022 The changing nature of Earth's reflected sunlight *Proc. R. Soc.* A **478** 20220053
[11] Huber M and Knutti R 2012 Anthropogenic and natural warming inferred from changes in Earth's energy balance *Nat. Geosci.* **5** 31–36
[12] Loeb N G, Doelling D R, Wang H, Su W, Nguyen C, Corbett J G, Liang L, Mitrescu C, Rose F G and Kato S 2018 Clouds and the earth's radiant energy system (CERES) energy balanced and filled (EBAF) top-of-atmosphere (TOA) edition-4.0 data product *J. Clim.* **31** 895–918
[13] Loeb N G, Mayer M, Kato S, Fasullo J T, Zuo H, Senan R, Lyman J M, Johnson G C and Balmaseda M 2022 Evaluating twenty-year trends in Earth's energy flows from observations and reanalyses *J. Geophys. Res. Atmos.* **127** e2022JD036686
[14] Kramer R J, He H, Soden B J, Oreopoulos L, Myhre G, Forster P M and Smith C J 2021 Observational evidence of increasing global radiative forcing *Geophys. Res. Lett.* **48** e2020GL091585
[15] Hersbach H *et al* 2020 The ERA5 global reanalysis *Q. J. R. Meteorol. Soc.* **146** 1999–2049
[16] Henderson G R, Barrett B S, Wachowicz L J, Mattingly K S, Preece J R and Mote T L 2021 Local and remote atmospheric circulation drivers of Arctic change: a review *Front. Earth Sci.* **9** 709896
[17] Serreze M C and Barry R G 2011 Processes and impacts of Arctic amplification: a research synthesis *Glob. Planet. Change* **77** 85–96
[18] Taylor P C, Boeke R C, Boisvert L N, Feldl N, Henry M, Huang Y, Langen P L, Liu W, Pithan F and Sejas S A 2022 Process drivers, inter-model spread, and the path forward: a review of amplified Arctic warming *Front. Earth Sci.* **9** 758361
[19] Peterson C A, Chen X, Yue Q and Huang X 2019 The spectral dimension of Arctic outgoing longwave radiation and greenhouse efficiency trends from 2003 to 2016 *J. Geophys. Res. Atmos.* **124** 8467–80
[20] Weatherhead E C, Reinsel G C, Tiao G C, Meng X L, Choi D, Cheang W K, Keller T, DeLuisi J, Wuebbles D J and Kerr J B 1998 Factors affecting the detection of trends: statistical considerations and applications to environmental data *J. Geophys. Res. Atmos.* **103** 17149–61
[21] Mlawer E J, Taubman S J, Brown P D, Iacono M J and Clough S A 1997 Radiative transfer for inhomogeneous atmospheres: RRTM, a validated correlated-k model for the longwave *J. Geophys. Res. Atmos.* **102** 16663–82
[22] Ramaswamy V, Collins W, Haywood J, Lean J, Mahowald N, Myhre G, Naik V, Shine K P, Soden B and Stenchikov G 2019 Radiative forcing of climate: the historical evolution of the radiative forcing concept, the forcing agents and their quantification, and applications *Meteorol. Monogr.* **59** 14.1–14.101
[23] Sherwood S C, Bony S, Boucher O, Bretherton C, Forster P M, Gregory J M and Stevens B 2015 Adjustments in the forcing-feedback framework for understanding climate change *Bull. Am. Meteorol. Soc.* **96** 217–28
[24] Huang Y 2013 On the longwave climate feedbacks *J. Clim.* **26** 7603–10
[25] Vial J, Dufresne J-L and Bony S 2013 On the interpretation of inter-model spread in CMIP5 climate sensitivity estimates *Clim. Dyn.* **41** 3339–62
[26] Soden B J, Held I M, Colman R, Shell K M, Kiehl J T and Shields C A 2008 Quantifying climate feedbacks using radiative kernels *J. Clim.* **21** 3504–20
[27] Shell K M, Kiehl J T and Shields C A 2008 Using the radiative kernel technique to calculate climate feedbacks in NCAR's Community atmospheric model *J. Clim.* **21** 2269–82
[28] Huang H and Huang Y 2023 Radiative sensitivity quantified by a new set of radiation flux kernels based on the ECMWF Reanalysis v5 (ERA5) *Earth Syst. Sci. Data* **15** 3001–21
[29] Huang Y, Tan X and Xia Y 2016 Inhomogeneous radiative forcing of homogeneous greenhouse gases *J. Geophys. Res. Atmos.* **121** 2780–9
[30] Chen Y-T, Huang Y and Merlis T M 2023 The global patterns of instantaneous CO_2 forcing at the top-of-atmosphere and surface *J. Clim.* **36** 6331–47
[31] Huang X 2020 *Aqua AIRS Level 3 Spectral Outgoing Longwave Radiation (OLR) Monthly* (Goddard Earth Sciences Data and Information Services Center (GES DISC)) (https://doi.org/10.5067/5P7KQ31XI7XJ)
[32] Huang Y and Shahabadi B 2014 Why logarithmic? A note on the dependence of radiative forcing on gas concentration: Huang & Bani Shahabadi *J. Geophys. Res. Atmos.* **119** 683–13,689
[33] Kiehl J Satellite detection of effects due to increased atmospheric carbon dioxide *Science* 1983 **222** 504–6
[34] Huang Y, Leroy S, Gero P J, Dykema J and Anderson J 2010 Separation of longwave climate feedbacks from spectral observations *J. Geophys. Res. Atmos.* **115** D7
[35] Blanchet J-P, Royer A, Châteauneuf F, Bouzid Y, Blanchard Y, Hamel J-F, de Lafontaine J, Gauthier P, O'Neill N T and Pancrati O 2011 TICFIRE: a far infrared payload to monitor the evolution of thin ice clouds *Proc. SPIE* **8176** 81761K
[36] L'Ecuyer T S, Drouin B J, Anheuser J, Grames M, Henderson D S, Huang X, Kahn B H, Kay J E, Lim B H and Mateling M 2021 The polar radiant energy in the far infrared experiment: a new perspective on polar longwave energy exchanges *Bull. Am. Meteorol. Soc.* **102** E1431–49
[37] Palchetti L, Brindley H, Bantges R, Buehler S, Camy-Peyret C, Carli B, Cortesi U, Del Bianco S, Di Natale G and Dinelli B 2020 unique far-infrared satellite observations

to better understand how Earth radiates energy to space *Bull. Am. Meteorol. Soc.* **101** E2030–46

[38] Held I M and Shell K M 2012 Using relative humidity as a state variable in climate feedback analysis *J. Clim.* **25** 2578–82

[39] Huang H, Huang Y, Wei Q and Hu Y Band-by-band spectral radiative kernels based on the ERA5 reanalysis *Sci. Data* 2024 **11** 237

[40] Huang H and Huang Y 2023 *Data for ERA5 Radiative Kernels* (Mendeley) (https://doi.org/10.17632/vmg3s67568)

[41] Huang H and Huang Y 2023 *Data for Spectral OLR Trend* (Mendeley) (https://doi.org/10.17632/wxdd574x8c)

[42] Doelling D R, Loeb N G, Keyes D F, Nordeen M L, Morstad D, Nguyen C, Wielicki B A, Young D F and Sun M 2013 Geostationary enhanced temporal interpolation for CERES flux products *J. Atmos. Ocean. Technol.* **30** 1072–90

[43] Lan X, T K W and Dlugokencky E J 2023 Trends in globally-averaged CH4, N2O, and SF6 determined from NOAA Global Monitoring Laboratory measurements. Version 2023–09 (https://doi.org/10.15138/P8XG-AA10)

[44] Lan X, Tans P and T K W 2023 Trends in globally-averaged CO2 determined from NOAA Global Monitoring Laboratory measurements. Version 2023–09 (https://doi.org/10.15138/9N0H-ZH07)